



Published in final edited form as:

Science. 2020 January 31; 367(6477): 580–586. doi:10.1126/science.aay6018.

N⁶-methyladenosine of chromosome-associated regulatory RNA regulates chromatin state and transcription

Jun Liu^{1,2,*}, Xiaoyang Dou^{1,2,*}, Chuanyuan Chen^{3,4,*}, Chuan Chen⁵, Chang Liu^{1,2}, Meng Michelle Xu⁶, Siqi Zhao^{3,4}, Bin Shen⁷, Yawei Gao^{5,†}, Dali Han^{3,4,8,9,†}, Chuan He^{1,2,10,†}

¹Department of Chemistry and Institute for Biophysical Dynamics, University of Chicago, Chicago, IL 60637, USA.

²Howard Hughes Medical Institute, University of Chicago, Chicago, IL 60637, USA.

³Key Laboratory of Genomic and Precision Medicine, Beijing Institute of Genomics, Chinese Academy of Sciences, Beijing 100101, China.

⁴College of Future Technology, Sino-Danish College, University of Chinese Academy of Sciences, Beijing 100049, China.

⁵Institute for Regenerative Medicine, Shanghai East Hospital, Shanghai Key Laboratory of Signaling and Disease Research, Frontier Science Center for Stem Cell Research, School of Life Sciences and Technology, Tongji University, Shanghai 200120, China.

⁶Department of Basic Medical Sciences, School of Medicine, Institute for Immunology, Beijing Key Laboratory for Immunological Research on Chronic Diseases, THU-PKU Center for Life Sciences, Tsinghua University, Beijing 100084, China.

⁷State Key Laboratory of Reproductive Medicine, Department of Histology and Embryology, Nanjing Medical University, Nanjing 211166, China.

⁸China National Center for Bioinformation, Beijing 100101, China.

⁹Institute for Stem Cell and Regeneration, Chinese Academy of Sciences, Beijing 100101, China.

¹⁰Department of Biochemistry and Molecular Biology, University of Chicago, Chicago, IL 60637, USA.

[†]Corresponding author. chuanhe@uchicago.edu (C.H.); handl@big.ac.cn (D.H.); gaoyawei@tongji.edu.cn (Y.G.).

*These authors contributed equally to this work.

Author contributions:

C.H., J.L., and Y.G. conceived the original idea and designed original studies. J.L. performed most experiments with help from Y.G., Chuan C., C.L., and M.M.X. X.D. performed most computational analyses with initial discovery of carRNA methylation by Chuanyuan C., S.Z., and D.H. B.S. constructed most mESC lines. J.L., X.D., and C.H. wrote the manuscript with input from all authors.

Competing interests: C.H. is a scientific founder and a member of the scientific advisory board of Accent Therapeutics, Inc.

Data and materials availability: All sequencing data have been deposited in Gene Expression Omnibus (GSE133600 and GSE140561). All other data are available in the manuscript or the supplementary materials.

SUPPLEMENTARY MATERIALS

science.sciencemag.org/content/367/6477/580/suppl/DC1

Materials and Methods

Supplementary Text

Figs. S1 to S23

Tables S1 and S2

References (29–44)

Abstract

*N*⁶-methyladenosine (m⁶A) regulates stability and translation of messenger RNA (mRNA) in various biological processes. In this work, we show that knockout of the m⁶A writer *Mettl3* or the nuclear reader *Ythdc1* in mouse embryonic stem cells increases chromatin accessibility and activates transcription in an m⁶A-dependent manner. We found that METTL3 deposits m⁶A modifications on chromosome-associated regulatory RNAs (carRNAs), including promoter-associated RNAs, enhancer RNAs, and repeat RNAs. YTHDC1 facilitates the decay of a subset of these m⁶A-modified RNAs, especially elements of the long interspersed element-1 family, through the nuclear exosome targeting-mediated nuclear degradation. Reducing m⁶A methylation by METTL3 depletion or site-specific m⁶A demethylation of selected carRNAs elevates the levels of carRNAs and promotes open chromatin state and downstream transcription. Collectively, our results reveal that m⁶A on carRNAs can globally tune chromatin state and transcription.

*N*⁶-methyladenosine (m⁶A) is an abundant modification on most eukaryote mRNAs (1, 2), regulated mainly by writer, eraser, and reader proteins (3). The mRNA m⁶A modification is installed by METTL3 (4) and can be removed by demethylases FTO and ALKBH5 (5, 6). Readers, including the YTH domain family and HNRNP proteins, directly or indirectly recognize the m⁶A-marked transcripts and affect mRNA metabolism (4, 7–9).

m⁶A plays critical roles in diverse biological processes, including the self-renewal and differentiation of embryonic and adult stem cells (3, 4). In mouse embryonic stem cells (mESCs), transcripts encoding pluripotency factors tend to be m⁶A-methylated and subjected to YTHDF2-mediated decay in cytoplasm, which affects their turnover during differentiation (10–12). However, m⁶A appears to also exhibit YTHDF2-independent regulations during early development, given that *Ythdf2* knockout (KO) mice can survive to late embryonic developmental stages but *Mettl3* KO results in early embryonic lethality (11, 13). Notably, mouse KO of the nuclear m⁶A reader *Ythdc1* exhibits similar early mouse embryonic lethality to the *Mettl3* KO (14). These observations imply that m⁶A could play additional roles in the nucleus that affect cell survival and differentiation. Previous studies have also suggested that m⁶A methylation on chromatin modifier transcripts or the chromosome binding of methyltransferase may affect transcription (15–17).

We investigated two independent *Mettl3* KO mESC lines (*Mettl3*^{-/-}-1 and *Mettl3*^{-/-}-2) (10) and analyzed newly transcribed RNA levels. *Mettl3* KO mESCs displayed marked increases in nascent transcripts synthesis compared with control wild-type (WT) mESCs (Fig. 1A). We generated stable rescue cell lines that express WT METTL3 or an inactive mutant METTL3 (fig. S1A). The increased transcription of nascent transcripts upon *Mettl3* KO was reversed with WT but not mutant METTL3 (Fig. 1B).

We next asked if the global chromatin state is affected by *Mettl3* deletion. We performed deoxyribonuclease (DNase) I-treated terminal deoxynucleotidyl transferase-mediated deoxyuridine triphosphate nick end labeling (TUNEL) assay and observed a notable increase in chromatin accessibility in *Mettl3* KO mESCs compared with wild type. Moreover, expression of WT but not mutant METTL3 reversed the increased chromatin accessibility, suggesting m⁶A dependence (Fig. 1, C and D).

We constructed conditional knockout (CKO) *Ythdc1* (fig. S1B) and *Ythdf2* (fig. S1C) mESCs. *Ythdc1* CKO showed a similar increase in transcription and chromatin openness as *Mettl3* KO (fig. S1, D and F), whereas *Ythdf2* CKO showed minimal differences (fig. S1, E and G). The changes observed in *Ythdc1* CKO mESCs were reversed by expressing WT but not mutant YTHDC1 (fig. S1, B, D, and F). Consistently, both H3K4me3 and H3K27ac, two histone marks associated with active transcription, were elevated upon *Mettl3* and *Ythdc1* depletion (fig. S1, H and I). Together, these data suggested a nuclear regulatory role for RNA m⁶A.

We next isolated nonribosomal RNAs from soluble nucleoplasmic and chromosome-associated fractions and quantified m⁶A/A by liquid chromatography–tandem mass spectrometry (LC-MS/MS) (fig. S2A). The m⁶A/A ratio in nonribosomal chromosome-associated RNAs (caRNAs) decreased the most (>50%) upon *Mettl3* KO (Fig. 2A and fig. S2B), suggesting an effect of m⁶A on caRNAs. We immunoprecipitated ribosomal-RNA–depleted, m⁶A-containing caRNAs and performed high-throughput sequencing (methylated RNA immunoprecipitation sequencing, MeRIP-seq) in *Mettl3* KO and WT mESCs. The m⁶A levels showed a global decrease after *Mettl3* KO (fig. S2C), consistent with LC-MS/MS analysis (Fig. 2A). We identified ~40,000 peaks in each sample; both m⁶A levels (fig. S2D) and peaks (fig. S2E) were fully reproducible. Compared with wild type, *Mettl3* KO samples showed more hypomethylated peaks (fig. S2F), with the largest reduction found at intergenic regions (fig. S2, G and H).

We analyzed three types of caRNAs with potential regulatory functions: promoter-associated RNA (paRNA), enhancer RNA (eRNA), and RNA transcribed from transposable elements (repeat RNA), which we termed chromosome-associated regulatory RNAs (carRNAs). The m⁶A levels of these carRNAs were markedly decreased in *Mettl3* KO mESCs (Fig. 2B). Approximately 15 to 30% of all carRNAs contain m⁶A in mESCs, ~60% of which are regulated by METTL3 (fig. S3A). These m⁶A peaks contain GAC and AAC motifs, similar to those of the coding mRNAs (fig. S3, B and C). We categorized carRNAs into m⁶A–marked and non-m⁶A subgroups and found that the abundances of m⁶A–marked transcripts, but not non-m⁶A RNAs, were significantly elevated upon *Mettl3* KO (Fig. 2C and fig. S3D). Additionally, changes in m⁶A levels negatively correlated with changes in expression levels for all three carRNA groups upon *Mettl3* KO (fig. S3E). Together, these data suggest that m⁶A methylation destabilizes these carRNAs.

Previous work has uncovered that YTHDC1 associates with components of the nuclear exosome targeting (NEXT) complex, which is responsible for degradation of certain non-coding nuclear RNAs (18). We confirmed that YTHDC1 interacts with the NEXT components RBM7 and ZCCHC8 (fig. S4A). Because YTHDC1 is a known m⁶A reader and *Ythdc1* CKO induced transcription up-regulation (fig. S1D), we hypothesized that YTHDC1 recognizes a subset of m⁶A–marked carRNAs and triggers their decay through NEXT in mESCs. Consistently, depletion of *Ythdc1* or *Zcchc8*, but not of *Ythdf2*, increased the m⁶A/A ratio of caRNAs (fig. S4B). We subsequently performed MeRIP-seq of nonribosomal caRNAs and observed consistently increased m⁶A levels after *Ythdc1* depletion (fig. S4, C to E). We identified more hypermethylated peaks in *Ythdc1* CKO mESCs compared with controls (fig. S4F). The distribution of m⁶A peaks on mRNA was not

notably altered (fig. S4G); however, the proportion of m⁶A peaks at intergenic regions increased upon *Ythdc1* CKO (fig. S4H). These observations suggest that YTHDC1, like METTL3, affects carRNAs transcribed mostly from intergenic regions.

We examined carRNAs and observed markedly increased m⁶A for repeat RNAs upon YTHDC1 depletion (fig. S5A). Specifically, ~20 to 30% of m⁶A-marked paRNAs and eRNAs and >60% of m⁶A-marked repeat RNAs are affected by YTHDC1 depletion, indicating a main role of YTHDC1 in affecting the stability of repeat RNAs in mESCs (fig. S5B). These m⁶A peaks in different regions share similar motifs to those we detected previously (fig. S5, C and D). Moreover, we correlated m⁶A fold changes on three carRNA groups separately and observed distinct negative correlations in all cases between *Mettl3* and *Ythdc1* depletion (fig. S5E), which further indicates that YTHDC1 promotes decay of a portion of these carRNAs. We next performed nuclear RNA decay assays and observed notably increased half lifetimes for all three groups of carRNAs upon *Ythdc1* CKO (Fig. 2D and fig. S5F). Moreover, the m⁶A-marked RNAs from all three carRNA groups showed greater increases in half lifetime compared with those of non-m⁶A RNAs after *Ythdc1* CKO (Fig. 2E and fig. S5G).

We then ranked repeats families according to their m⁶A peak enrichment fold changes in response to *Mettl3* or *Ythdc1* depletion and identified the long interspersed element-1 (LINE1) family as one of the most responsive in both cases (fig. S6, A and B). LINE1 elements are the most abundant class of mouse retrotransposon, transcribed in early embryos, and they play critical roles in development—particularly in remodeling chromatin structure and regulating transcription (19, 20). We observed that m⁶A levels of each subfamily of LINE1 negatively correlate with their divergence: younger LINE1 contains higher m⁶A levels (fig. S6, C and D) and shows more significant methylation fold changes (fig. S6, E and F) upon *Mettl3* or *Ythdc1* depletion. We next verified that the decay of LIMd_F, a representative young subfamily of LINE1, is regulated by YTHDC1 and METTL3 in an m⁶A-dependent manner (supplementary text and figs. S6G and S7).

paRNAs, eRNAs, and repeat RNAs, such as LINEs, can regulate transcription by affecting chromatin architecture at corresponding genomic loci. Because *Mettl3* KO increases both transcription and chromatin accessibility (Fig. 1), we next examined whether these changes are regulated by methylation of these carRNAs. We performed time-course RNA sequencing of nascent transcripts as well as total nuclear RNAs and conducted mammalian native elongating transcript sequencing (mNET-seq) (21, 22) in *Mettl3* KO and WT mESCs. Both the global expression level (Fig. 3, A and B) and transcription rate (Fig. 3, C and D, and fig. S8, A and B) increased upon *Mettl3* KO. Genes that were up-regulated in *Mettl3* KO mESCs tended to have upstream carRNAs marked with m⁶A more frequently than those that were down-regulated (Fig. 3, A and B). Moreover, genes with m⁶A-marked upstream carRNAs attained higher increases in transcription rate than those with non-m⁶A-marked upstream carRNAs. The same is true when sorting genes with their precursor mRNAs (pre-mRNAs) not subjected to m⁶A methylation (Fig. 3, E to F, and fig. S8, C to E), which indicates that the reduced m⁶A methylation of these carRNAs upon *Mettl3* KO activates the transcription of downstream genes.

Notably, we found that all m⁶A-dependent genes that showed reduced upstream carRNA methylation upon *Mettl3* depletion (~6584 genes) exhibited increased transcription rates (Fig. 3G). We identified a subset of these genes that demonstrated transcription rate differences >1 upon *Mettl3* KO (fig. S9A) and found that these genes are mainly involved in transcription regulation, chromatin modification, and stem cell population maintenance (fig. S9B). Hence, the reduced m⁶A methylation of carRNAs not only promotes downstream transcription but may activate genes involved in chromatin opening, initiating a positive feedback loop. We further analyzed *Prdm9*, *Kmt2d* (encoding two H3K4me3 methyltransferases), *Esrrb*, and *Ranbp17* (related with differentiation), all of which possess upstream carRNAs with reduced m⁶A level upon *Mettl3* KO (fig. S10). Consistently, the half lifetime of these carRNAs and the transcription rate of their downstream genes both increased upon *Mettl3* KO, and these changes could be rescued by WT but not mutant METTL3 (fig. S11).

The interactions between super-enhancers and their target genes are known to be affected by transcription of exosome-regulated transcripts in mESCs (23). We examined super-enhancers and found that ~80% of super-enhancer RNAs (seRNAs) contain m⁶A peaks (Fig. 3H and fig. S12A). The m⁶A methylation level of seRNAs decreased (fig. S12, B and C) and the m⁶A-marked seRNAs showed a greater increase in abundances compared with non-m⁶A-marked ones upon *Mettl3* KO (Fig. 3I). seRNAs that showed reduced m⁶A level upon *Mettl3* KO were associated with increased transcription rates at downstream genes (Fig. 3J); genes with transcription rate differences larger than one were mainly involved in transcription regulation, chromatin modification, and stem cell maintenance (fig. S12, D and E), consistent with results obtained from other carRNAs (fig. S9). Moreover, we found that genes regulated by m⁶A-marked upstream seRNAs tended to exhibit greater increases in transcription rate than those regulated by m⁶A-marked upstream typical eRNAs upon *Mettl3* KO (fig. S12F).

We next investigated chromatin state changes affected by altered carRNA methylation. We performed chromatin immunoprecipitation sequencing (ChIP-seq) and observed global increases of these two active marks, H3K4me3 and H3K27ac, upon *Mettl3* KO (fig. S13, A and B), consistent with the Western blot results (fig. S1H). Moreover, genes with m⁶A-marked upstream carRNAs showed greater increases in H3K4me3 and H3K27ac than genes with non-m⁶A upstream carRNAs in *Mettl3* KO mESCs (Fig. 4A). Likewise, *Mettl3* KO mESCs showed obvious increases in both marks at regions that flank METTL3-enriched DNA loci (fig. S13, C and D). These data suggested that stabilizing the upstream carRNAs in *Mettl3* KO mESCs could increase the deposition of active histone marks.

We suspect that carRNAs could recruit proteins, such as CBP/EP300 and YY1, to promote open chromatin and activate transcription (24, 25). In fact, YY1 was identified as one of the top enriched transcription factors (TFs) at genomic regions that harbor m⁶A-marked carRNAs (fig. S14A). Our ChIP-seq experiments revealed global increases of EP300 and YY1 binding in *Mettl3* KO mESCs (Fig. 4, B and C), which correlated well with higher nearby eRNAs or paRNAs abundances (fig. S14, B and C). Moreover, both EP300 and YY1 binding negatively correlate with the m⁶A level of nearby carRNAs (Fig. 4, D and E), and *Mettl3* KO leads to elevated EP300 and YY1 binding at regions that lose m⁶A (Fig. 4, F and

G). The genomic regions with both m⁶A-marked carRNAs and binding of EP300 or YY1 showed the greatest increase in H3K27ac compared with regions with just m⁶A or just EP300/YY1 binding upon *Mettl3* KO (Fig. 4H). We also performed ChIP-seq of JARID2, a component of the polycomb repressive complex 2 (PRC2), because RNA transcripts could repel PRC2 binding to maintain chromatin openness (26). We observed a globally decreased JARID2 binding, correlating well with the abundance increases of eRNAs and repeats transcripts upon *Mettl3* KO (fig. S14, D and E). Furthermore, JARID2 tends to bind to regions with high m⁶A methylation of carRNAs (fig. S14F), with a positive correlation between the m⁶A level on carRNA and local JARID2 binding changes upon *Mettl3* KO (fig. S14G). Therefore, these m⁶A-regulated carRNAs may stabilize the open chromatin state by not only recruiting active TFs but also repelling repressive factors, such as PRC2, upon loss of methylation.

Lastly, elevated LINE1 may also modulate global chromatin accessibility (19). We blocked LINE1 RNA in *Mettl3*^{-/-} mESCs and observed an overall reduction in chromatin accessibility (Fig. 4I) (20). We employed a fused CRISPR-dCas13b system (27) with either WT or inactive mutant FTO (fig. S15A). Only when targeting LINE1 by guide RNA (gRNA) with dCas13b-*wt* FTO, but not dCas13b-*mu* FTO, did we observe decreased m⁶A level and increased half lifetime for LINE1, together with a globally increased chromatin accessibility (fig. S15, B to E). We then applied the dCas13b-FTO system to genes that harbor m⁶A-marked upstream carRNAs (fig. S16). When targeting carRNAs using gRNAs and dCas13b-*wt* FTO, we observed site-specific methylation reduction, with little methylation change observed using dCas13b-*mu* FTO or negative control gRNAs (Fig. 4J and fig. S17). We also observed increased half lifetime of these carRNAs, up-regulation of downstream gene transcription, and elevated local H3K4me3 and H3K27ac levels (Fig. 4J and fig. S18). Together, these results strongly support our discovery that m⁶A methylation of carRNAs controls carRNA stability and downstream gene transcription.

To explore functional relevance of this m⁶A-mediated regulation, we modulated the LINE1 RNA level in WT and *Mettl3* KO mESCs. LINE1 abundance was elevated in *Mettl3* KO mESCs (fig. S19A) (11). Blocking LINE1 elevated differentiation capacity and decreased cell renewal in *Mettl3* KO mESCs (fig. S19, B to D). In contrast, targeting LINE1 using gRNA with dCas13b-*wt* FTO resulted in decreased differentiation capacity and increased cell renewal in WT mESCs but not with Cas13b-*mu* FTO (fig. S19, B to D). We also confirmed regulatory functions of m⁶A-marked carRNAs in endometrial cancer progression, in which down-regulation of METTL3 increases cell proliferation, migration, and tumor growth (supplementary text and figs. S20 to S23) (28).

In this work, we report that carRNAs can be m⁶A methylated by METTL3. A subset of these m⁶A-marked carRNAs (mainly LINE1 repeats) is destabilized by YTHDC1 via the NEXT complex. We show that m⁶A serves as a switch to affect abundances of these carRNAs, thus tuning nearby chromatin state and downstream transcription (Fig. 4K). Effects of m⁶A methylation on carRNAs could vary; m⁶A may stabilize modified carRNAs in different cell types. In mESCs, the transcription activation induced by m⁶A depletion is coupled with the increased chromatin accessibility, enrichment of certain TFs, and elevated histone marks, revealing a direct cross-talk between carRNA m⁶A methylation and chromatin state. Our

findings demonstrate an additional layer of regulatory effect of carRNA m⁶A on transcription.

Supplementary Material

Refer to Web version on PubMed Central for supplementary material.

ACKNOWLEDGMENTS

We thank H. Chang for *Mettl3* KO mESCs and J. Tauler and A. Andersen from Life Science Editor for editing.

Funding: This study was supported by the National Institute of Health HG008935 to C.H.; Strategic Priority Research Program XDA16010506 to D.H.; National Key R&D Program of China 2018YFA0109700 to D.H.; National Institute of Health ES030546 to C.H.; National Key R&D Program of China 2016YFA0100400 to Y.G. and Chuan C.; the China Scholarship Council (CSC) for the visit of Y.G. to the University of Chicago; National Science Fund for Excellent Young Scholars 31922017 to D.H.; and the CAS Hundred Talent Program to D.H. The Mass Spectrometry Facility of the University of Chicago is funded by the National Science Foundation (CHE-1048528). C.H. is an investigator of the Howard Hughes Medical Institute.

REFERENCES AND NOTES

1. Dominissini D et al., *Nature* 485, 201–206 (2012). [PubMed: 22575960]
2. Meyer KD et al., *Cell* 149, 1635–1646 (2012). [PubMed: 22608085]
3. Frye M, Harada BT, Behm M, He C, *Science* 361, 1346–1349 (2018). [PubMed: 30262497]
4. Roundtree IA, Evans ME, Pan T, He C, *Cell* 169, 1187–1200 (2017). [PubMed: 28622506]
5. Jia G et al., *Nat. Chem. Biol* 7, 885–887 (2011). [PubMed: 22002720]
6. Zheng G et al., *Mol. Cell* 49, 18–29 (2013). [PubMed: 23177736]
7. Wang X et al., *Nature* 505, 117–120 (2014). [PubMed: 24284625]
8. Wang X et al., *Cell* 161, 1388–1399 (2015). [PubMed: 26046440]
9. Xiao W et al., *Mol. Cell* 61, 507–519 (2016). [PubMed: 26876937]
10. Batista PJ et al., *Cell Stem Cell* 15, 707–719 (2014). [PubMed: 25456834]
11. Geula S et al., *Science* 347, 1002–1006 (2015). [PubMed: 25569111]
12. Wang Y et al., *Nat. Cell Biol* 16, 191–198 (2014). [PubMed: 24394384]
13. Ivanova I et al., *Mol. Cell* 67, 1059–1067.e4 (2017). [PubMed: 28867294]
14. Kasowitz SD et al., *PLOS Genet.* 14, e1007412 (2018). [PubMed: 29799838]
15. Wang Y et al., *Nat. Neurosci* 21, 195–206 (2018). [PubMed: 29335608]
16. Barbieri I et al., *Nature* 552, 126–131 (2017). [PubMed: 29186125]
17. Slobodin B et al., *Cell* 169, 326–337.e12 (2017). [PubMed: 28388414]
18. Lubas M et al., *Mol. Cell* 43, 624–637 (2011). [PubMed: 21855801]
19. Jachowicz JW et al., *Nat. Genet* 49, 1502–1510 (2017). [PubMed: 28846101]
20. Percharde M et al., *Cell* 174, 391–405.e19 (2018). [PubMed: 29937225]
21. Mayer A et al., *Cell* 161, 541–554 (2015). [PubMed: 25910208]
22. Nojima T et al., *Cell* 161, 526–540 (2015). [PubMed: 25910207]
23. Pefanis E et al., *Cell* 161, 774–789 (2015). [PubMed: 25957685]
24. Bose DA et al., *Cell* 168, 135–149.e22 (2017). [PubMed: 28086087]
25. Sigova AA et al., *Science* 350, 978–981 (2015). [PubMed: 26516199]
26. Wang X et al., *Nat. Struct. Mol. Biol* 24, 1028–1038 (2017). [PubMed: 29058709]
27. Rauch S, He C, Dickinson BC, *J. Am. Chem. Soc* 140, 11974–11981 (2018). [PubMed: 30183280]
28. Liu J et al., *Nat. Cell Biol* 20, 1074–1083 (2018). [PubMed: 30154548]

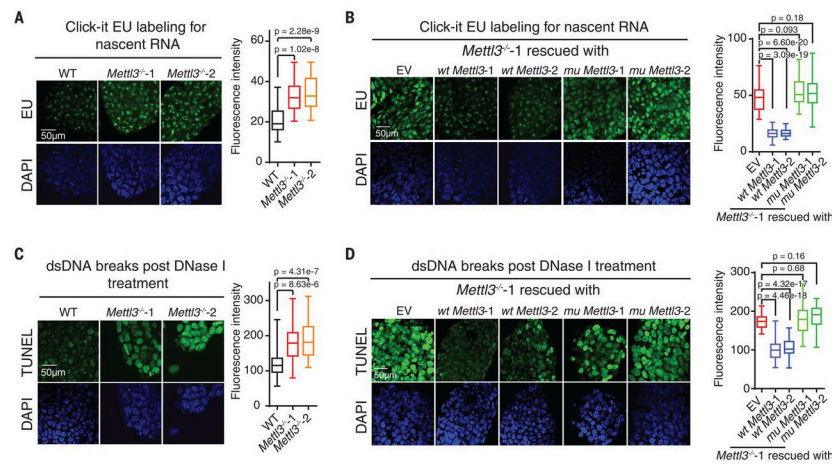


Fig. 1. *Mettl3* KO in mESCs leads to increased nascent RNA transcription and chromatin accessibility.

(A and B) Analysis of nascent RNA synthesis in WT or *Mettl3*^{-/-} mESCs [(A), *Mettl3*^{-/-1} and -2 are two independently generated KO lines], and *Mettl3*^{-/-} mESCs rescued with WT or an inactive mutant *Mettl3* (B). Nascent RNA synthesis was detected by using a click-it RNA Alexa fluor 488 imaging kit. EU, 5-ethynyl uridine; DAPI, 4',6-diamidino-2-phenylindole. (C and D) Analysis of chromatin accessibility in WT or *Mettl3*^{-/-} mESCs (C), and *Mettl3*^{-/-} mESCs rescued with WT or mutant *Mettl3* (D). DNase I-treated TUNEL assay was performed. For (A) to (D), the nucleus is counterstained by DAPI. EV (empty vector) refers to *Mettl3*^{-/-} mESCs when transfected with empty vector plasmid. dsDNA, double-stranded DNA.

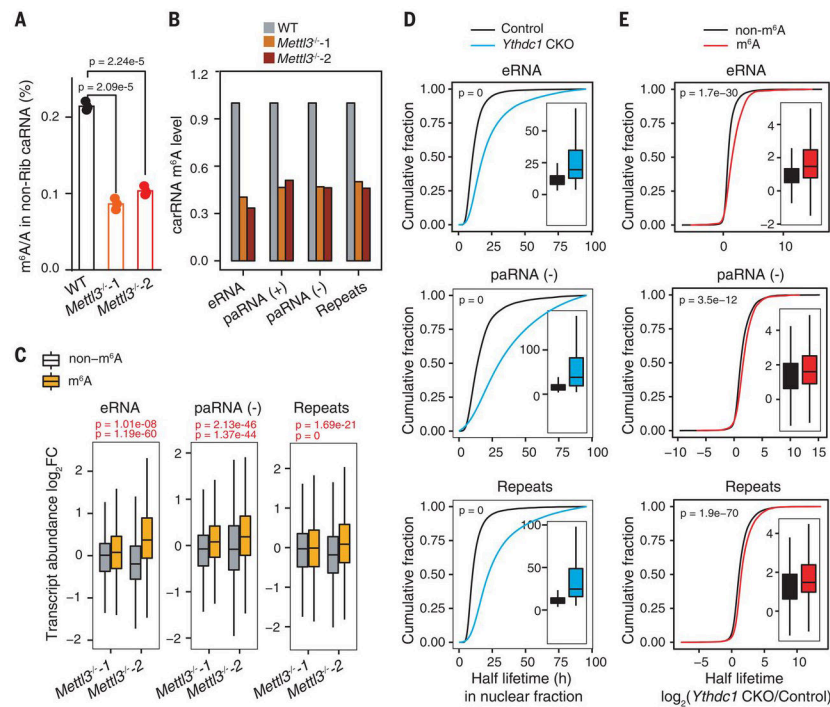


Fig. 2. Transcript turnover of carRNAs is regulated by m⁶A.

(A) LC-MS/MS quantification of the m⁶A/A ratio in nonribosomal (non-Rib) caRNAs (including pre-mRNA) extracted from WT or *Mettl3*^{-/-} mESCs. *n* = 3 biological replicates; error bars indicate means ± SEM. (B) m⁶A level changes on carRNAs were quantified through normalizing m⁶A sequencing results with spike-in between WT and *Mettl3* KO mESCs. *n* = 2 biological replicates. (C) carRNAs were divided into methylated (m⁶A) or nonmethylated (non-m⁶A) groups. The boxplot shows greater increases in transcript abundance fold changes of the m⁶A group versus the non-m⁶A group upon *Mettl3* KO over WT mESCs. For (A) and (C), *P* values were determined by two-tailed *t* test. (D) Cumulative distribution and boxplots (inside) of nuclear carRNA half lifetime changes in CKO *Ythdc1* and control mESCs. (E) Cumulative distributions and boxplots (inside) of the half lifetime changes of carRNAs upon *Ythdc1* CKO. carRNAs were divided into methylated (m⁶A) or nonmethylated (non-m⁶A) groups. Depletion of YTHDC1 led to greater half lifetime increases of m⁶A-marked carRNAs than non-m⁶A-marked ones. For (D) and (E), *P* values were calculated by a nonparametric Wilcoxon-Mann-Whitney test. h, hours.

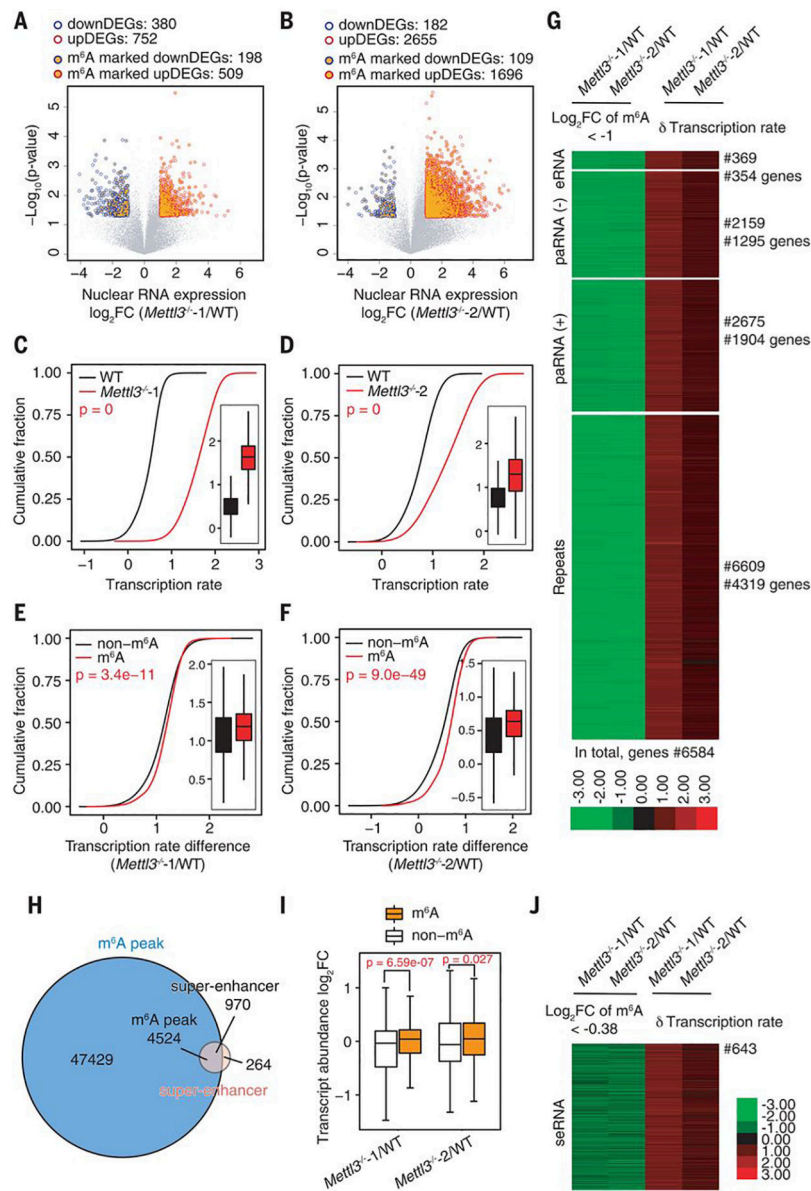


Fig. 3. The m⁶A level of carRNAs affects downstream gene expression and transcription rate. (A and B) Volcano plot of genes with differential expression levels in *Mettl3*⁻¹ (A) or *Mettl3*⁻² (B) versus WT mESCs [$P < 0.05$ and $|\log_2FC| > 1$ (FC, fold change)]. Genes with upstream, m⁶A-marked carRNAs are shown with orange circles. Gene expression level was normalized to ERCC spike-in with linear regression method. DEG, differentially expressed gene. (C and D) Cumulative distribution and boxplot (inside) of gene transcription rate in *Mettl3*⁻¹ (C) or *Mettl3*⁻² (D) versus WT mESCs. (E and F) Cumulative distribution and boxplot (inside) of transcription rate difference between *Mettl3*⁻¹ (E) or *Mettl3*⁻² (F) versus WT mESCs. Genes were categorized into two subgroups according to whether their upstream carRNAs contain m⁶A (m⁶A) or not (non-m⁶A). For (C) to (F), P values were calculated by a nonparametric Wilcoxon-Mann-Whitney test. (G) Heatmap showing the m⁶A level fold changes ($\log_2FC < -1$) on carRNAs and downstream gene

transcription rate difference between *Mettl3* KO and WT mESCs. **(H)** Venn diagram showing the overlap between the m⁶A peaks and super-enhancer peaks in mESCs. **(I)** Boxplot showing fold changes of the abundance of m⁶A-marked and non-m⁶A-marked seRNAs between *Mettl3*^{-/-} and WT mESCs. For (A), (B), and (I), *P* values were determined by two-tailed *t* test. **(J)** Heatmap showing fold change ($\log_2\text{FC} < -0.38$) of m⁶A level of seRNAs and transcription rate difference of their downstream genes between *Mettl3* KO and WT mESCs.

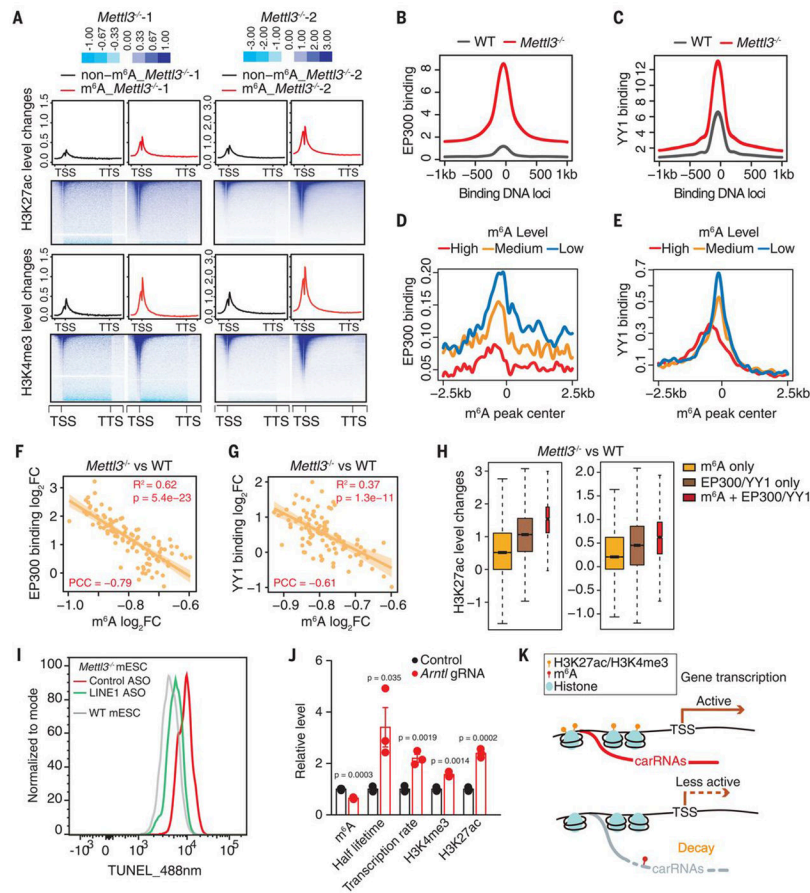


Fig. 4. The m⁶A level of carRNAs affects local chromatin state and downstream transcription. (A) Profiles of H3K27ac (top) and H3K4me3 (bottom) level changes on gene body together with 2.5 kb upstream of the TSS (transcription start site) and 2.5 kb downstream of the TTS (transcription termination site) in WT and *Mettl3* KO mESCs. Genes were categorized into two groups according to whether they harbor upstream m⁶A-marked carRNAs (m⁶A) or not (non-m⁶A). (B and C) Profiles of EP300 (B) or YY1 (C) DNA binding at their peak center and flanking 2.5 kb regions in WT and *Mettl3* KO mESCs. (D and E) Profiles of EP300 (D) and YY1 (E) DNA binding at the center of m⁶A peaks overlapped with carRNAs and its flanking 2.5 kb regions in WT mESCs. m⁶A peaks were categorized into highly (high), moderately (medium), or lowly (low) methylated groups, according to their m⁶A levels in WT mESCs. (F and G) The correlation between changes in m⁶A level of the carRNAs and changes in EP300 (F) or YY1 (G) DNA binding at genomic regions that show m⁶A differences with *Mettl3* KO. The genomic regions were categorized into 100 bins on the basis of fold change rank of m⁶A level upon *Mettl3* KO. (H) Barplots showing H3K27ac level changes at genomic regions that are m⁶A methylated (m⁶A only, without EP300 and YY1 binding), bound by EP300 or YY1 (EP300/YY1 only, without m⁶A carRNA), and m⁶A methylated with EP300 and YY1 binding (m⁶A + EP300/YY1). The last group showed the highest increase upon *Mettl3* KO. (I) Analysis of chromatin accessibility in *Mettl3* KO mESCs treated with control or LINE1 antisense oligos (ASOs). DNase I-treated TUNEL assay was performed. (J) A dCas13b-FTO (WT or inactive mutant) construct with gRNA

targeting the seRNA of *Arntl* was used to reduce the m⁶A level of *Arntl* seRNA. After treatment, increased half lifetime of the target seRNA, elevated local H3K27ac and H3K4me3 levels, and increased *Arntl* transcription rate were observed, accompanied by the decreased seRNA m⁶A level. **(K)** A schematic model showing how m⁶A affects transcription by regulating the decay of upstream carRNAs stability and chromatin state.

Author Manuscript

Author Manuscript

Author Manuscript

Author Manuscript